A theoretical study of rotational diffusion models for rod-shaped viruses

The influence of motion on ^{31}P nuclear magnetic resonance lineshapes and transversal relaxation

Pieter C. M. M. Magusin and Marcus A. Hemminga
Department of Molecular Physics, Agricultural University, Dreijenlaan 3, 6703 HA Wageningen, The Netherlands

ABSTRACT Information about the interaction between nucleic acids and coat proteins in intact virus particles may be obtained by studying the restricted backbone dynamics of the incapsulated nucleic acids using ^{31}P nuclear magnetic resonance (NMR) spectroscopy. In this article, simulations are carried out to investigate how reorientation of a rod-shaped virus particle as a whole and isolated nucleic acid motions within the virion influence the ^{31}P NMR lineshape and transversal relaxation dominated by the phosphorus chemical shift anisotropy. Two opposite cases are considered on a theoretical level. First, isotropic rotational diffusion is used as a model for mobile nucleic acids that are loosely or partially bound to the protein coat. The effect of this type of diffusion on lineshape and transversal relaxation is calculated by solving the stochastic Liouville equation by an expansion in spherical functions. Next, uniaxial rotational diffusion is assumed to represent the mobility of phosphorus in a virion that rotates as a rigid rod about its length axis. This type of diffusion is approximated by an exchange process among discrete sites. As turns out from these simulations, the amplitude and the frequency of the motion can only be unequivocally determined from experimental data by a combined analysis of the lineshape and the transversal relaxation. In the fast motional region both the isotropic and the uniaxial diffusion model predict the same transversal relaxation as the Redfield theory. For very slow motion, transversal relaxation resembles the nonexponential relaxation as observed for water molecules undergoing translational diffusion in a magnetic field gradient. In this frequency region T_{2e} is inversely proportional to the cube root of the diffusion coefficient. In addition to the isotropic and uniaxial diffusion models, a third model is presented, in which fast restricted nucleic acid backbone motions dominating the lineshape are superimposed on a slow rotation of the virion about its length axis, dominating transversal relaxation. In an accompanying article the models are applied to the ^{31}P NMR results obtained for bacteriophage M13 and tobacco mosaic virus.

INTRODUCTION

Phosphorus nuclear magnetic resonance (NMR) spectroscopy is a powerful technique for obtaining information about structure and dynamics of the nucleic acid backbone in intact bacteriophages and plant viruses. As all phosphorus nuclei belong to the viral genome, information about the nucleic acid backbone can be obtained selectively, even though the virus particles largely consist of proteins. Indeed, during the last 15 years ^{31}P NMR studies of various viruses have appeared in the literature. In one class of studies, rapidly tumbling, mostly spherical viruses, such as the plant viruses alfalfa mosaic virus, cowpea mosaic virus, tomato bushy stunt virus, and the bacteriophages Qβ and MS2, have been investigated in dilute solution by use of high resolution NMR spectroscopy (1–4). In these studies conclusions about the dynamic behavior of the nucleic acids inside the virions have been drawn from linewidths and relaxation times. In other studies, solid-state NMR techniques have been used to record ^{31}P spectra of viruses in more concentrated solutions or viscous gels, such as tomato bushy stunt virus and the rod-shaped tobacco mosaic virus (TMV) and the bacteriophages Pf1 and fd (3, 5–8). From qualitative lineshape analyses conclusions were drawn about motional frequencies and amplitudes, which agree with the general picture evolved from dilute solution studies: nucleic acids inside virions do not undergo large amplitude motions at frequencies higher than 10^4 Hz and motional lineshape effects observed in dilute solutions can be explained by overall motion of the viral particle as a rigid body.

To interpret our ^{31}P NMR results for bacteriophage M13 and plant virus TMV in more detail, we have carried out simulations of the ^{31}P lineshape and transversal relaxation for various types of diffusion with intermediate motional frequencies and amplitudes. As for phosphorus nuclei in biomolecular systems such simulations have been carried out for phospholipid membrane systems (9, 10), but not for nucleic acids encapsulated in viruses. Several diffusion models can be constructed to explain the motional effects observed by NMR spectroscopy. On the one hand, as in general a virion is a complex structure of a nucleic acid molecule situated within a protein coat, the observed ^{31}P lineshape and transversal relaxation may actually reflect a superposition of many types of motion, such as overall rotation of the virus particle as a whole and isolated backbone motions of the nucleic acid inside. All these motions together may influence the lineshape and relaxation decay in a way roughly comparable with random rotational diffusion in a viscous solution. Similar assumptions were made in ^{31}P NMR studies of DNA in solution (11, 12). In this article, an isotropic diffusion model is set up and the effects of this type of diffusion on the lineshape and transversal relaxation will be presented. On the other hand, one may

Address correspondence to M. A. Hemminga, Department of Molecular Physics, Agricultural University, P.O. Box 8128, 6700 ET Wageningen, The Netherlands.

try to interpret the motional effects observed in ^{31}P NMR spectra and transversal relaxation in terms of rigid body motion. For rod-shaped viruses of the size of filamentous phages (~ 1 μm length and 9 nm diameter) in water, diffusion coefficients in the order of 10^4 and 10^1 Hz can be calculated for diffusion about the length axis and of the length axis itself (13). Rigid body rotation of these rod-shaped viruses is thus well approximated by uniaxial diffusion about the length axis. To show the effect of this type of diffusion, we construct a uniaxial diffusion model. In addition, we use alternative simulation methods to check the limiting behavior of the isotropic and the uniaxial diffusion model for fast and very slow diffusion. In both diffusion models one single type of motion is assumed to influence both the lineshape and transversal relaxation. In general, the observed lineshape and transversal relaxation may be dominated by different motions. To study such a case we will test a simple model, which combines slow motion of the virion as a whole with fast motion of the phosphodiesters inside. The application of these simulation models to the experimental data will be treated in an accompanying article (14). In this article we present the theory of the simulations and discuss the outcome and trends therein in a general manner.

THEORY

In the presence of only Zeeman interaction, anisotropic chemical shift, and rotational diffusion, ^{31}P lineshapes and transversal relaxation can be described by the positive and negative-helicity components $\mu_\pm(\Omega, t)\mathbf{I}_\pm$ of the spin density operator $\rho(\Omega, t)$, where Ω denotes the orientation of the principal axis system of the chemical shift tensor in a laboratory frame with the z-axis parallel to the magnetic field, t represents the time, and $\mathbf{I}_+$ and $\mathbf{I}_-$ are the raising and lowering operators for a spin-½ nucleus. By assumption, the detected NMR signal is proportional to the positive-helicity component integrated over all shift tensor orientations

$$\mu_+(t) = \int d\Omega \mu_+(\Omega, t). \tag{1}$$

The positive and negative-helicity components obey part of the stochastic Liouville equation (10, 15)

$$\frac{d\mu_\pm(\Omega, t)}{dt} = (\pm i\omega(\Omega) + \Gamma_\Omega)\mu_\pm(\Omega, t), \tag{2}$$

where $\omega(\Omega)$ denotes the combined Zeeman and orientation-dependent chemical shift interaction and Γ_Ω is the stochastic operator representing a specific type of rotational diffusion. Combining Eq. 1 with the formal solution of Eq. 2 and assuming isotropic spin density at $t = 0$, $\mu_\pm(\Omega, 0) = \mu_0$ (e.g., after a nonselective pulse), it follows that the normalized free induction decay (FID) $S(t)$ is given by

$$S(t) = \frac{\mu_+(t)}{\mu_+(0)} = \frac{\int d\Omega e^{(i\omega(\Omega)+\Gamma_\Omega)t}\mu_0}{\int \mu_0 \, d\Omega}. \tag{3}$$

As a π pulse interchanges the positive and negative-helicity component, an echo produced by a π pulse at time τ is given at a time $2\tau + t$ by

$$E(2\tau, t) = \frac{\mu_+(2\tau + t)}{\mu_+(0)} = \frac{\int d\Omega e^{(i\omega(\Omega)+\Gamma_\Omega)(\tau+t)}e^{(-i\omega(\Omega)+\Gamma_\Omega)\tau}\mu_0}{\int \mu_0 \, d\Omega}, \tag{4}$$

(16). A "powder average" relaxation decay, i.e., the spatial average relaxation curve of all orientations, is defined for a series of τ values by setting $t = 0$ in Eq. 4. Although Eqs. 3 and 4 are formally correct, an appropriate method for dealing with the exponential operators therein should be used to actually calculate free induction and relaxation decays. However, already from these formal solutions it can be derived for many types of motion, including the ones discussed in this article, that motion does not change the second moment of the lineshape and causes nonexponential transversal relaxation, which contradicts what is often assumed (17–19). This contradiction becomes clear when Eqs. 3 and 4 are expanded as Taylor series in t and τ, respectively.

For types of diffusion which are nonorienting, i.e., lead to an isotropic distribution of spin density, and which cannot create or annihilate net spin density, although they can, of course, change "local" spin density, the diffusion operator Γ_Ω satisfies the mathematical conditions $\Gamma_\Omega 1 = 0$, where 1 denotes the isotropic distribution, and $\langle \Gamma_\Omega f(\Omega) \rangle = 0$ for any distribution function $f(\Omega)$. For example, for restricted diffusion, the latter condition ensures that no loss of spin density occurs at the boundaries. Any type of motion that fulfils both conditions may be shown to change only third and higher order terms in the Taylor series of the calculated free induction decays and relaxation decays, as derived from Eqs. 3 and 4

$$S(t) = S_0(t) + 2Bt^3 + \cdots, \tag{5a}$$

and

$$E(2\tau, 0) = 1 - B(2\tau)^3 + \cdots, \tag{5b}$$

with

$$B = -\frac{\int d\Omega \omega(\Omega)\Gamma_\Omega\omega(\Omega)}{12\int d\Omega}, \tag{5c}$$

where $S_0(t)$ denotes the FID in the absence of diffusion. The constant B in Eqs. 5a, 5b, and 5c is positive, so that

relaxation curves actually decay (sufficiently close to $t = 0$) and lineshapes are narrowed by motion. Eqs. 5a and 5b further indicate that diffusion does not change the second moment of the lineshape and transversal relaxation is nonexponential. Obviously, this does not agree with the common, experimentally confirmed assumption that fast motion modulates the second moment of a lineshape and causes exponential relaxation. However, higher order terms in the Taylor series become dominant at larger values of t or τ, especially for fast motions, which may mask this disagreement and reduce it to a purely theoretical detail. Although Taylor series provide some information about lineshape moments and relaxation decays close to $t = 0$, they are not easily applicable to simulate motional effects completely. Instead, we have used different approaches, which will be explained in more detail below.

Isotropic diffusion

The effect of isotropic diffusion on ^{31}P lineshapes and relaxation decays can be calculated by introducing the spin density operator $\rho(\Omega, t)$ as a function of the chemical shift tensor orientation $\Omega = (\alpha, \beta, \gamma)$ relative to the laboratory frame and calculating this density as a function of orientation and time. The specific form of Eq. 2 for isotropic diffusion is

$$\frac{d\mu_{\pm}(\Omega, t)}{dt} = (\pm i\omega(\Omega) - \mathrm{D}\nabla^2_{\Omega})\mu_{\pm}(\Omega, t), \qquad (6)$$

with the combined Zeeman and orientation dependent chemical shift interaction expressed in terms of the Wigner functions $D^2_{m'm}(\alpha\beta\gamma) = \exp(im'\gamma)d^2_{m'm}(\beta) \times \exp(im\alpha)$ (20, 21) as

$$\omega(\Omega) = \omega_0 + \omega_0\sigma_0 + \omega_0 F_0 D^2_{00}(\Omega) + \omega_0 F_2(D^2_{20}(\Omega) + D^2_{-20}(\Omega)), \qquad (7)$$

where $\omega_0 = \gamma B_0$ is the Zeeman angular frequency, $\sigma_0 = (\sigma_{11} + \sigma_{22} + \sigma_{33})/3$ is the isotropic shift, $F_0 = (\sigma_{33} - \sigma_0)$ is the anisotropy parameter, and $F_2 = (\sigma_{22} - \sigma_{11})/\sqrt{6}$ characterizes the asymmetry of the chemical shift tensor with Cartesian components σ_{11}, σ_{22}, and σ_{33}. Isotropic diffusion is represented in Eq. 3 by the differential operator

$$\mathrm{D}\nabla^2_{\Omega} = \frac{\mathrm{D}\partial}{\sin\beta\partial\beta}\left(\sin\beta\frac{\partial}{\partial\beta}\right) + \frac{\mathrm{D}}{\sin^2\beta}\frac{\partial^2}{\partial\gamma^2}, \qquad (8)$$

where D denotes the diffusion coefficient. Utilizing the method of Freed (9, 15) Eq. 6 is solved by making an expansion of the two transversal spin density components in Wigner functions $D^l_{m'm}(\Omega)$ being eigenfunctions of the diffusion operator. In contrast with the usual procedure, however, we carry out our simulations in the time domain, because the calculation of free induction decays can be more easily extended to the calculation of echoes and transversal relaxation decays.

As follows from Eqs. 7 and 8, the chemical shift and the diffusion operator are independent of α and invariant under the rotations $\gamma \rightarrow \pi \pm \gamma$ and $\beta \rightarrow \pi - \beta$. Therefore, if initial spin density is homogeneously distributed over all tensor orientations, $\mu_{\pm}(\Omega, 0) = \mu_0 D^0_{00}(\Omega)$, spin density bears the same symmetry at all times and may thus be expanded more compactly in terms of the normalized eigenfunctions $\sqrt{(4l+1)/8\pi^2}(D^{2l}_{-2m'0}(\Omega) + D^{2l}_{2m'0}(\Omega))$. Neglecting terms with l larger than a specific value L and substituting the expansion in Eq. 6, this equation reduces to a matrix equation of the order $N = (L+1)(L+2)/2$, the formal solution of which is

$$\mu_+(t) = e^{\mathbf{M}t}\mu_+(0) \qquad (9a)$$

and

$$\mu_-(t) = e^{\mathbf{M}^*t}\mu_-(0), \qquad (9b)$$

where $\mu_+(t)$ and $\mu_-(t)$ have been redefined as vectors containing the N expansion components of the positive and negative-helicity component, respectively, the matrix $\mathbf{M}$ contains the couplings among the coefficients in $\mu_+(t)$, and $\mathbf{M}^*$ is the complex conjugate of $\mathbf{M}$. To calculate the FID the positive-helicity component must be integrated over all tensor orientations (Eq. 1). All expansion terms vanish under this integration, except for the first, isotropic term. If initial spin density is homogeneously distributed over all tensor orientations, as assumed earlier, the normalized FID $S(t)$ is proportional to the "upper-left" element of the exponential matrix

$$S(t) = (e^{\mathbf{M}t})_{11}, \qquad (10)$$

(see Eq. 3) where the exponential matrix is calculated by diagonalizing $\mathbf{M}$. It follows from Eqs. 9a and 9b that a π pulse, which interchanges the positive and negative-helicity component at time τ, produces an echo given at time $2\tau + t$ by

$$E(2\tau, t) = (e^{\mathbf{M}(\tau+t)}e^{\mathbf{M}^*\tau})_{11}, \qquad (11)$$

(see Eq. 4). Fourier transformation of a calculated FID or echo produces the corresponding lineshape. A powder average decay can be calculated for a series of τ values using Eq. 11 by setting $t = 0$. Note that in this case the product matrix of the two exponential matrices is hermitian, so that its diagonal elements are real and the transversal decay is purely absorptive.

Uniaxial diffusion

In the uniaxial diffusion model the orientation of the principal axis system of the chemical shift tensor is specified by the Euler angles $\Omega' = (\alpha, \beta, \gamma)$ in a coordinate system fixed in a rotor, representing the virion. The orientation of this rotor axis system in the laboratory frame, in turn, is given by $\Omega'' = (\phi, \theta, \psi)$. In an isotropic powder, the rotors are randomly oriented with respect to the magnetic field. The number of relative chemical shift tensor orientations within the virion may vary from a single one

in Pf1 or three in TMV to a large value representing a nucleic acid backbone without structural correlation to the viral coat geometry, like bacteriophage fd (5, 8). In this model it is assumed that there is an isotropic distribution of relative chemical shift tensor orientations inside the virion. By introducing the spin density operator $\rho(\Omega'', \Omega', t)$, the specific form of Eq. 2 for rotor diffusion is

$$\frac{d\mu_{\pm}(\Omega'', \Omega', t)}{dt} = (\pm i\omega(\Omega'', \Omega') + \Gamma_{\psi})\mu_{\pm}(\Omega'', \Omega', t), \quad (12)$$

with the combined Zeeman and chemical shift interaction

$$\begin{aligned}\omega(\Omega'', \Omega') &= \omega_0 + \omega_0\sigma_0 + \omega_0 \\ &\times \sum_{m'=-2}^{2} D^2_{m'0}(\Omega'')[F_0 D^2_{0m'}(\Omega') \\ &+ F_2(D^2_{2m'}(\Omega') + D^2_{-2m'}(\Omega'))] \\ &= \omega_0 + \omega_0\sigma_0 + \omega_0 \\ &\times \sum_{m'=-2}^{2} d^2_{m'0}(\theta)[F_0 d^2_{0m'}(\beta) + F_2(d^2_{2m'}(\beta)e^{2i\gamma} \\ &+ d^2_{-2m'}(\beta)e^{-2i\gamma})]e^{im'(\psi+\alpha)}, \end{aligned} \quad (13)$$

where the parameters are explained in Eq. 7. For uniaxial diffusion restricted to angles $\psi \in [\psi_o - \lambda, \psi_o + \lambda]$, the diffusion operator Γ_{ψ} in Eq. 12 is defined on this interval as

$$\Gamma_{\psi} = D\frac{\partial^2}{\partial\psi^2} + DB_{\psi}(\psi_o, \lambda), \quad (14)$$

where $D(\partial^2/\partial\psi^2)$ denotes the free uniaxial diffusion operator (10) and $B_{\psi}(\psi_o, \lambda)$ is a boundary operator, which vanishes everywhere except at the edges and ensures that Γ_{ψ} fulfils the conditions $\Gamma_{\psi}1 = 0$ and $\langle \Gamma_{\psi} f(\Omega) \rangle = 0$ (see above). It follows from the symmetry properties of Eqs. 12, 13, and 14 that, if spin density is homogeneously distributed over all rotor orientations and the relative tensor orientations at time $t = 0$, $\mu_{\pm}(\Omega'', \Omega', t)$ are independent of ϕ at any time. Furthermore, as α and ψ are rotation angles about the same axis, there is no way to distinguish between α-diffusion, ψ-diffusion, or a combination of both and $\mu_{\pm}(\Omega'', \Omega', t)$ should be a function of $\psi + \alpha$ rather than of ψ and α separately. By redefining the average angle ψ_o as $\langle \psi + \alpha \rangle$ and the fluctuating angle ψ as $\psi + \alpha - \psi_o$ and collecting the nonfluctuating angles in $\Theta = (\theta, \psi_o, \beta, \gamma)$ the notation for the spin density components can be changed to $\mu_{\pm}(\Theta, \psi, t)$.

Following the procedure of Dufourc et al. (10), we solve Eq. 12 by using a finite-difference approximation of the diffusion operator. To simulate the effect of uniaxial diffusion restricted by $\pm\lambda$ on the positive-helicity component, N discrete values ψ_n are taken from the interval $[-\lambda, +\lambda]$ with a constant difference δ between subsequent values. Exchange among these N orientations is calculated from the coupled equations for $2 < n < N - 1$

$$\begin{aligned}\frac{d\mu_{+}(\Theta, \psi_n, t)}{dt} &= \frac{D}{\delta^2}\mu_{+}(\Theta, \psi_{n-1}, t) \\ &+ \left(i\omega(\Theta, \psi_n) - \frac{2D}{\delta^2}\right)\mu_{+}(\Theta, \psi_n, t) \\ &+ \frac{D}{\delta^2}\mu_{+}(\Theta, \psi_{n+1}, t), \end{aligned} \quad (15a)$$

combined with the equations for the boundaries

$$\begin{aligned}\frac{d\mu_{+}(\Theta, \psi_1, t)}{dt} &= \left(i\omega(\Theta, \psi_1) - \frac{D}{\delta^2}\right)\mu_{+}(\Theta, \psi_1, t) \\ &+ \frac{D}{\delta^2}\mu_{+}(\Theta, \psi_2, t) \end{aligned} \quad (15b)$$

$$\begin{aligned}\frac{d\mu_{+}(\Theta, \psi_N, t)}{dt} &= \frac{D}{\delta^2}\mu_{+}(\Theta, \psi_{N-1}, t) \\ &+ \left(i\omega(\Theta, \psi_N) - \frac{D}{\delta^2}\right)\mu_{+}(\Theta, \psi_N, t). \end{aligned} \quad (15c)$$

For free rotor diffusion we take $\lambda = \pi$ and connect the boundaries by defining exchange between ψ_N and ψ_1. By combination of the N components in the vector $\mu_{+}(\Theta, \Psi, t)$ and the shift and the diffusion factors in the symmetric matrix $\mathbf{M}$ Eq. 12 may be rewritten as a matrix equation, the formal solution of which is

$$\mu_{+}(\Theta, t) = e^{\mathbf{M}t}\mu_{+}(\Theta, 0). \quad (16a)$$

Also here the analogous solution for the negative-helicity component is simply

$$\mu_{-}(\Theta, t) = e^{\mathbf{M}^*t}\mu_{-}(\Theta, 0). \quad (16b)$$

Because the FID is proportional to the positive-helicity component, Eq. 16a must be summed over all orientations (Eq. 1). If at $t = 0$ all orientations have the same spin density, i.e., $\mu_{+}(\Theta, 0) = \mu_o(1, 1, \ldots, 1, 1)$, the normalized contribution $S(\Theta, t)$ to the FID by N diffusion-coupled orientations for a specific combination of static angles Θ is

$$S(\Theta, t) = \frac{1}{N}\sum_{i,j}(e^{\mathbf{M}t})_{ij}, \quad (17)$$

where the exponential matrix is calculated by diagonalizing $\mathbf{M}$ (see Appendix). A π pulse at time τ produces an echo given at time $2\tau + t$ by

$$E(\Theta, 2\tau, t) = \frac{1}{N}\sum_{i,j}(e^{\mathbf{M}(\tau+t)}e^{\mathbf{M}^*\tau})_{ij}. \quad (18)$$

A way to calculate Eq. 18 efficiently is discussed in the Appendix. To simulate a FID, an echo or an average transversal decay curve of a powder of randomly oriented rotors, Eqs. 17 and 18 should be integrated for all rotor orientations (θ, ψ_o) and summed over all internal chemical shift tensor orientations (β, γ). Fourier transformation of a simulated FID or echo produces the corresponding lineshape. Like for isotropic diffusion the

decay of transversal coherence is purely absorptive due to the hermitian character of the product matrix of the two exponential matrices in Eq. 18.

Ultra-slow and fast diffusion

For very slow and fast diffusion matrix calculations as discussed above are not necessary and faster simulation procedures can be used instead. Here we discuss such alternative procedures, because they provide independent checks for the limiting behavior of the isotropic and uniaxial diffusion models. For very slow diffusion with a diffusion coefficient D much smaller than the inhomogeneous linewidth $|\omega_o(\sigma_{33} - \sigma_{11})|$, the lineshape is hardly influenced by motion and can well be calculated following one of the standard procedures for simulating static lineshapes (21). If the diffusion coefficient is even smaller than the average motion-induced homogeneous linewidth, transversal relaxation may also be calculated in an alternative way. In this case it may be assumed that within a time that the echo intensity decays to typically e^{-1} of its initial value, spin density mainly spreads out to orientations close to its initial orientation. As a consequence the variation of chemical shift as a function of orientation is well approximated by a "local" linear or bilinear field gradient. It has been derived earlier that the Hahn echo in a linear field gradient G decays in a nonexponential way as $\exp(-DG^2t^3/12)$ (19, 22). Similarly we find for ultra-slow uniaxial diffusion (neglecting boundary effects in the case of restricted diffusion)

$$E(t, 0) = \frac{\int d\Omega \int d\Omega' \exp(-D(\partial\omega/\partial\psi)^2 t^3/12)}{\int d\Omega \int d\Omega'}, \quad (19a)$$

and for ultra-slow isotropic diffusion

$$E(t, 0) = \frac{\int d\Omega \exp(-D\{(\partial\omega/\partial\beta)^2 + (\sin\beta)^{-2}(\partial\omega/\partial\gamma)^2\} t^3/12)}{\int d\Omega}. \quad (19b)$$

Eqs. 19a and 19b show that the transversal decay $E(t, 0)$ can generally be described as $F(Dt^3)$, where $F(x)$ is some nonexponential, decaying function independent of D. For this decay of the echo produced by a single π pulse, a transversal relaxation time T_{2e} may be empirically defined by fitting a single exponential to the curve. If $F(x)$ reaches the value e^{-1} for a specific value of x, defined as x_o, T_{2e} should be approximately $(x_o/D)^{1/3}$. Obviously, in the ultra-slow motion region T_{2e} is inversely proportional to the cube root of D.

For fast diffusion the lineshape may be calculated from the time-averaged expression $\langle\omega\rangle$ for ω. Under fast isotropic diffusion chemical shift anisotropy is averaged to $\langle\omega\rangle = \omega_0 + \omega_0\sigma_0$ and the lineshape becomes lorentzian with a linewidth $1/(\pi T_2)$. In contrast, fast uniaxial diffusion does not completely average the chemical shift anisotropy. Replacing the complex exponentials in Eq. 13 by their average value $\exp\{im'(\psi + \alpha)\}\,\mathrm{sinc}(m'\lambda)$ on the interval $\langle\psi + \alpha - \lambda, \psi + \alpha + \lambda\rangle$, where $\mathrm{sinc}(m'\lambda)$ denotes $\sin(m'\lambda)/(m'\lambda)$, one obtains the average chemical shift expression for fast rotor diffusion with restriction half-angle λ as

$$\langle\omega(\Omega'', \Omega')\rangle = \omega_0 + \omega_0\sigma_0 + \omega_0 \sum_{m'=-2}^{2} d^2_{m'0}(\theta)[F_0 d^2_{0m'}(\beta) + F_2(d^2_{2m'}(\beta)e^{2i\gamma} + d^2_{-2m'}(\beta)e^{-2i\gamma}) e^{im'(\psi+\alpha)}\,\mathrm{sinc}(m'\lambda). \quad (20)$$

From Eq. 20 the lineshape may be simulated numerically by calculating $\langle\omega\rangle$ for a large number of combinations ($\cos\theta$, $\psi + \alpha$, $\cos\beta$, γ).

In the limit of short correlation times, T_{2e} may be calculated using the Redfield approximation, which relates T_{2e} to the spectral density. The general equation for the transversal relaxation for a chemical shift tensor undergoing axially symmetric diffusion is

$$1/T_{2e} = (1/40)(\omega_0 F_0)^2 \sum_{i=0}^{2} c_i(\Omega)\{3J_i(\omega_0) + 4J_i(0)\}, \quad (21)$$

where $c_i(\Omega)$ are geometric parameters relating the principle axis systems of the diffusion and the chemical shift tensors, and $J_i(\omega)$ are the spectral density functions $2\tau_i/(1 + \omega^2\tau_i^2)$, with correlation times τ_i depending on the diffusion model (23). In the case of isotropic diffusion $\tau_0 = \tau_1 = \tau_2 = 1/(6D)$ and $\langle c_0(\Omega) + c_1(\Omega) + c_2(\Omega)\rangle = (1 + \eta^2/3)$, so that for correlation times shorter than T_{2e} but larger than $1/\omega_o$, the general equation simply reduces to

$$T_{2e} = \frac{6D}{M_2}, \quad (22a)$$

where M_2 is the second moment of the static lineshape: $(1/5)(\omega_o F_o)^2(1 + \eta^2/3)$. For uniaxial diffusion of a rotor containing many randomly oriented shift tensors inside, $J_0(\omega) = 0$, $\tau_1 = 1/D$, $\tau_2 = 1/(4D)$, and $\langle c_1(\Omega)\rangle = \langle c_2(\Omega)\rangle = (2/5)(1 + \eta^2/3)$. This may be substituted into Eq. 21 to show that for $D \ll \omega_o$

$$T_{2e} = \frac{2D}{M_2}. \quad (22b)$$

To use Eq. 21 for restricted diffusion the spectral density functions should be modified in a rather complicated way (24). Instead, T_{2e} may be approximately calculated from a more simple equation, which for short correlation times relates T_{2e} to the portion ΔM_2 of the second lineshape moment M_2 that is modulated by the motion

$$\frac{1}{T_{2e}} = \Delta M_2 \tau, \quad (23)$$

(17, 18). Theoretically Eq. 23 disagrees with Eq. 5, because, as discussed above, the latter implicates that diffu-

sion does not change the second moment. From Eq. 20, however, which we derived neglecting the time-dependent part of ω, a second moment can be calculated for fast uniaxial diffusion, which does vary as a function of the restriction angle

$$M_2(\lambda) = M_2(0)\{(1/5) + (2/5)\,\mathrm{sinc}^2(2\lambda) + (2/5)\,\mathrm{sinc}^2(2\lambda)\}, \quad (24)$$

where $M_2(0)$ is the second moment of the static lineshape (see Eq. 22a). From Eq. 24, ΔM_2 may be calculated as $M_2(0) - M_2(\lambda)$. The occurrence of only one correlation time in Eq. 23 provides another inconsistency: two correlation times are necessary for unrestricted uniaxial diffusion and for the restricted case the correlation function is multiexponential. Often, however, $\tau = 1/(6D)$ is used as "the" correlation time of unrestricted uniaxial diffusion (10). Substitution of ΔM_2 and τ into Eq. 23 then yields

$$T_{2e} = \frac{6D}{(2/5)M_2(0)\{2 - \mathrm{sinc}^2(\lambda) - \mathrm{sinc}^2(2\lambda)\}}. \quad (25)$$

For free uniaxial diffusion, i.e., for $\lambda \to \infty$, Eq. 25 predicts a higher value for T_{2e} than Eq. 22b. Interestingly, the two equations would match if the average of the two correlation times used in the derivation of Eq. 22b, $(\tau_1 + \tau_2)/2 = 5/(8D)$, were taken for τ. Both variants will be compared with the outcome of simulations using the uniaxial diffusion model (see below).

Combined diffusion

In the combined diffusion model nucleic acid backbone motion, represented by very fast, restricted ψ or α-diffusion, is superimposed on top of slow, free ψ-diffusion, representing overall rotation of the virion as a whole. The approach is the same as for the uniaxial diffusion model (see above), except that Eq. 20 is used instead of Eq. 13. The effect of the superimposed diffusion is thus merely a pseudostatic reduction of the chemical shift anisotropy. In principle, both the fast restricted and the slow free diffusion influence the lineshape and transversal relaxation. It is assumed in this model, however, that the overall diffusion is too slow to effect the lineshape, whereas the superimposed, restricted diffusion is so fast, that it only has an indirect effect on transversal relaxation by scaling the chemical shift anisotropy in a pseudostatic way. Under these conditions the lineshape is dominated by the fast, restricted motion and transversal relaxation by the slow overall diffusion.

METHODS

All simulations were carried out on a μVAX and a VAX workstation VS2000 (Digital Equipment Corp., Maynard, MA) using self-made Fortran programs as described in Theory. The double-precision complex IMSL routine EIGCC (IMSL Inc., Houston, Texas) was employed for matrix diagonalization. Lineshapes and powder average transversal relaxation decays presented here were simulated for ^{31}P at 121.5 MHz with relative chemical shift tensor values $\sigma_{11} - \sigma_o = 77$ ppm, $\sigma_{22} - \sigma_o = 18$ ppm, and $\sigma_{33} - \sigma_o = -95$ ppm. For simulations of isotropic diffusion, the number of expansion terms was taken as high as necessary for lineshapes and relaxation curves not to change any more upon a further increase. The exact number depended on the diffusion coefficient D put into the calculation, but for D = 5 kHz as a typical example, the expansion was truncated after 45 terms. For the other diffusion models a random distribution of rotor orientations with respect to the magnetic field and a random distribution of relative chemical shift tensor orientations within the virion were assumed. The number of angles θ, β, γ between 0 and $\pi/2$, ψ_o between 0 and 2π and ψ between $-\lambda$ and λ (see Theory and Appendix) was taken high enough to observe no change upon a further increase and depended on the diffusion coefficient D and the restriction halfangle λ. Typically for a simulation using the uniaxial diffusion model with D = 50 kHz and $\lambda = 1.25$ rad 10 values each for $\cos\theta$ and ψ_o, 5 values each for $\cos\beta$ and γ, and 12 ψ values were taken into account. Except for the simulations of the fast diffusion lineshapes, all simulations were carried out in the time domain. Lineshapes were obtained by Fourier transformation after multiplication with an exponential function corresponding to 1 kHz linebroadening, in analogy with the processing of experimental data. For the nonexponential powder average decays, a T_{2e} value was defined by fitting a single exponential to the calculated decay (11), which differs from the e^{-1} definition by Woessner et al. (25), but is closer to the analysis of experimental decays in practice.

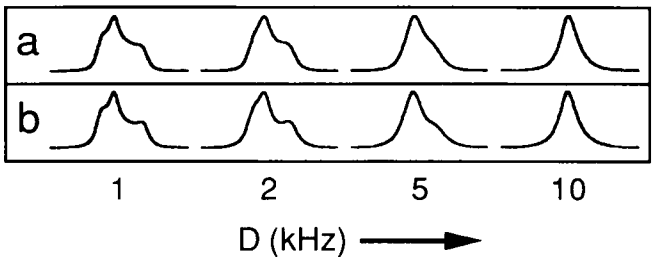

FIGURE 1 Fourier transformed free induction decays (*a*) and echoes at $2\tau = 60\ \mu$s (*b*) for isotropic diffusion with a diffusion coefficient of 1, 2, 5, and 10 kHz.

DISCUSSION

Isotropic diffusion

Fig. 1 shows the lineshape effect of isotropic diffusion with a diffusion coefficient increasing from 1 to 10 kHz: discontinuities get increasingly less pronounced and the resonance line narrows more and more. Discontinuities tend to be more pronounced in echo spectra than in FID spectra caused by T_{2e} anisotropy or, in particular, the first derivatives of the chemical shift to β and γ being zero at these positions (Eq. 19b). For fast diffusion, $D \geq 10$ kHz, powder average decays of transversal coherence are practically indistinguishable from single exponentials (not shown), which agrees with Redfield's relaxation theory for fast motions. Below 10 kHz, however, the simulated relaxation decays are significantly nonexponential, as expected from Eq. 5b, and T_{2e} values defined by least-square fitting a single exponential to the simulated decay depend on the time domain sampled

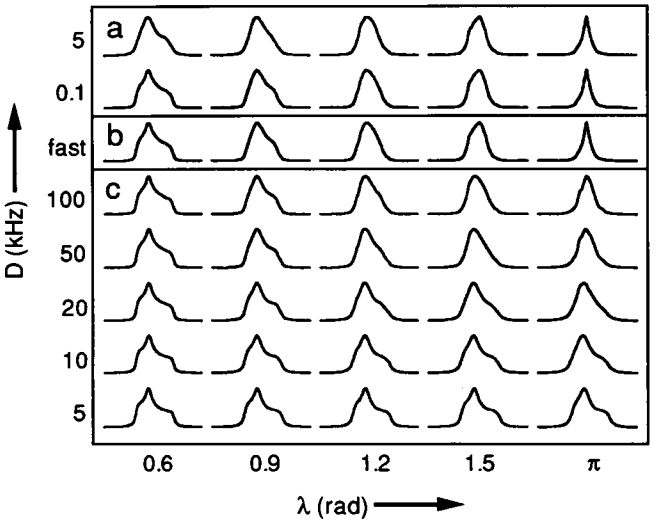

FIGURE 2 Fourier transformed echoes at $2\tau = 60\ \mu s$ for the three types of uniaxial diffusion with various coefficients and restriction angles: (*a*) combined diffusion, (*b*) fast diffusion, and (*c*) intermediate diffusion.

(see Fig. 3 *a*). In general, for fast motions Redfield theory predicts T_2 to become longer at increasing mobility and the opposite trend is proposed for slow motions (19). Indeed, our calculations show that for an increasing diffusion coefficient D, T_{2e} first decreases as a linear function of the cube root of D, and then passes through a minimum for D = 5 kHz and finally becomes proportional to D. A similar trend has been calculated by Woessner et al. (25). Instead of the cube root dependence in the slow motion region, Pauls et al. (17) have suggested that for a process of large rotational jumps among discrete sites T_{2e} would be inversely proportional to the jumping rate ($\approx$D). However, in their jumping model only spin density leaving the sites is taken into account and the contribution of spin density arriving at the sites is neglected, so that the corresponding jumping operator Γ does not fulfill the condition $\Gamma 1 = 0$ (Eqs. 5a and 5b). In an attempt to find an empirical formula for T_{2e} as a function of D, it was found that the curves in Fig. 3 *a* fit well to $T_{2e} = \{(aD^{-1/3})^c + (bD)^c\}^{1/c}$, where parameters *a* and *b* determine the limiting behavior for slow and fast motion, respectively, and parameter *c* defines the "sharpness" of the transition between the two limits. As a consequence of this hyperbolic correlation, an experimentally observed T_{2e} above the minimum value can be interpreted in two ways and a lineshape analysis is necessary to decide between the two. For slow diffusion up to 1 kHz plots of echo decays $E(t, 0)$ versus Dt^3 are independent of D, as expected from the linear field gradient approximation (Eq. 19b). This also explains the cube root dependence of T_{2e} on D in the slow-motion region. In the fast-motion region chemical shift anisotropy relaxation can be calculated alternatively from $T_2 = 6D/M_2$ (Eq. 22a). As shown in Fig. 3 *a* this agrees well with the simulation results for fast diffusion, which proves that the isotropic diffusion model is consistent with Redfield theory.

Uniaxial diffusion

The influence of uniaxial diffusion on ^{31}P lineshapes and relaxation curves has been calculated for various restriction half-angles and diffusion coefficients (Figs. 2 *c* and 3 *d*). Hardly any lineshape effect is observed for rotor diffusion with coefficients below 10^4 Hz or restriction half-angles below 0.5 rad. For diffusion coefficients larger than 10^5 Hz, the lineshape does not change upon a further increase and above a half-angle of π rad; the lineshapes are indistinguishable from free rotor diffusion lineshapes at the same diffusion coefficients. In contrast with the simulated lineshape for isotropic diffusion, the lineshapes of Fourier transformed free induction decays differ only slightly from the corresponding echoes at 60 μs, probably as a consequence of the random orientation of shift tensors with respect to the rotor axis in this model.

Powder average T_{2e} values have been obtained by fitting the simulated echo decays to a single exponential. In Fig. 3 *b* these T_2 values are plotted versus the diffusion

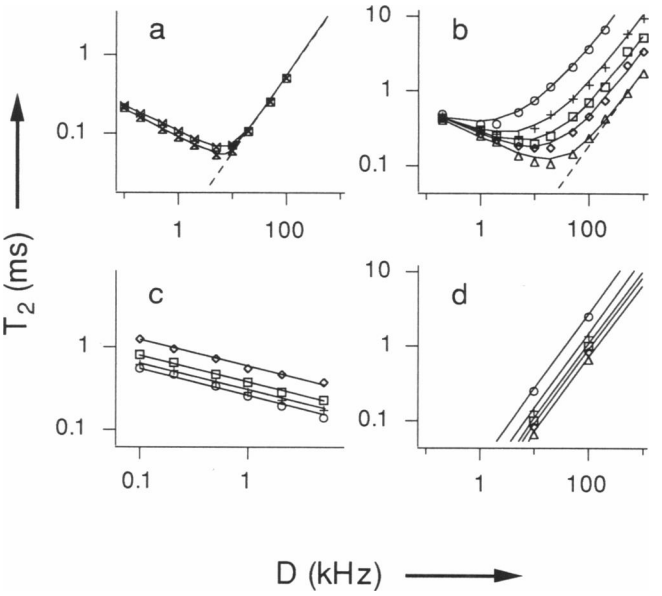

FIGURE 3 T_{2e} values as a function of the diffusion coefficients for (*a*) isotropic diffusion, (*b*) uniaxial diffusion, (*c*) combined diffusion and (*d*) fast diffusion. For isotropic diffusion (*a*) T_{2e} values obtained by fitting a single exponential to the powder average decay up to a time of 0.8 ms (⋈) and 1.6 ms (⧖) are shown in the same plot for comparison. For the uniaxial and combined diffusion model the presented T_{2e} values are obtained by fitting up to 0.8 and 1.6 ms, respectively, for various restriction half-angles: 0.6 rad (○), 0.9 rad (+), 1.2 rad (□), 1.5 rad (◇), and π rad (△). For the fast diffusion model T_{2e} was calculated from Eq. 25. The broken lines in *a* and *b* represent the T_{2e} values calculated using the Redfield approximation for isotropic diffusion (Eq. 22a) and free uniaxial diffusion (Eq. 22b), respectively.

coefficients for a number of restriction angles. Similarly as for isotropic diffusion, the curves fit well to $T_{2e} = \{(aD^{-1/3})^c + (bD)^c\}^{1/c}$. Thus, for slow motion T_{2e} is inversely proportional to the cube root of D, reaches a minimum value in the intermediate region, and is proportional to D for fast motions. Again we find for slow diffusion that plots of echo decays $E(t, 0)$ versus Dt^3 are independent of D and that Eq. 19a provides a good approximation, which explains the cube root dependence of T_{2e} on D in the slow-motion region. For fast, unrestricted diffusion about a single axis, T_{2e} may be calculated alternatively from $T_{2e} = 2D/M_2$ (Eq. 22b). This agrees well with the outcome of the simulations for fast diffusion with restriction half-angle π (Fig. 3 *b*).

Fig. 3 *b* also shows the effects of motional amplitude on T_{2e}. For a given diffusion coefficient, T_{2e} decreases as the restriction angle becomes larger, but for coefficients below 1 kHz the curves in Fig. 3 *b* start to coincide. Apparently, for ultraslow diffusion the fraction of spin density that actually reaches the boundaries within a time comparable to T_{2e} is neglectable. In contrast, for fast motion the curves are well resolved. Relaxation curves simulated for a restriction half-angle of π are indistinguishable from free rotor relaxation curves.

The presence of the restriction half-angle λ as another fitting parameter beside the diffusion coefficient D complicates the interpretation of experimental data. A continuous set of parameter pairs (D, λ) share the same T_{2e} value (Fig. 3 *b*), so that the observed transversal relaxation can be interpreted in many ways, especially when noise hides detailed features of the relaxation curve. Likewise, a continuous set of (D, λ) lineshapes can be simulated that fit to the experimental line equally well. Even the theoretical lineshape simulated for free diffusion at 20 kHz is hard to distinguish from the one simulated for D = 50 kHz and λ = 1.5 rad (Fig. 2 *c*). Obviously, only a combined analysis of lineshape and transversal relaxation must be used to unequivocally interpret the data.

Fast uniaxial diffusion

Fast diffusion lineshapes, calculated from Eq. 20, correspond well to the lineshapes simulated for fast diffusion using the uniaxial diffusion model (Fig. 2 *b*). Clearly, the neglect of the time dependent part of ω from which Eq. 20 was derived is allowed in the fast frequency region. In contrast, T_{2e} values calculated from Eq. 25 do not match the values simulated for uniaxial diffusion. The order of magnitude, however, is the same and the tendency of increasing T_{2e} with decreasing λ is comparable. Given the earlier discussed inconsistency between Eqs. 5a and 23 on a theoretical basis, the similarity between the outcome of the two methods is striking. The alternative variant of Eq. 25, derived by taking $\tau = 5/(8D)$, does not provide a better approximation, except for $\lambda > 1$ rad. In the analysis of experimental data the fast diffusion model can be useful to make a quick estimation of the motional amplitude and frequency.

Combined diffusion

Utilizing the combined diffusion model, lineshapes and relaxation decays have been simulated for several combinations of internal restriction half-angles λ and overall diffusion coefficients D. For coefficients below 5 kHz lineshapes are hardly influenced by slow overall diffusion, but only depend on the internal restriction angles (Fig. 2 *a*). Slow overall diffusion does, however, influence transversal relaxation (Fig. 3 *d*). In the frequency region up to 5 kHz investigated, T_{2e} is inversely proportional to the cube root of D, as expected for ultraslow diffusion. In contrast to the T_{2e} trend observed in the uniaxial diffusion simulations, where T_{2e} shortens as the restriction half-angle λ increases, the combined diffusion model predicts that T_{2e} becomes larger at increasing λ, because internal motions with larger amplitudes average the shift anisotropy to a larger extend and thereby reduce the chemical shift fluctuations caused by overall diffusion more. The curves for λ = 0.6 and 0.9 rad in Fig. 3 *c* almost coincide, indicating that very fast, internal motion with amplitudes below 1 rad hardly influence T_{2e}. Clearly, under these circumstances transversal relaxation is dominated by the overall diffusion alone.

In the strategy for interpreting experimental results in terms of combined diffusion, the first step is the determination of the internal restriction angle from the lineshape using the fast diffusion model. Then, for this restriction angle the overall diffusion coefficient can be obtained from an analysis of the relaxation curve using the combined diffusion model. This procedure of extracting λ from the experimental lineshape first and then D from the observed relaxation curve is much less time consuming than a "two-dimensional" searching procedure necessary to unequivocally determine λ and D using the uniaxial diffusion model discussed above.

CONCLUSION

In summarizing the simulation results discussed above, it is convenient to divide motional amplitudes into three ranges. Small amplitude motions do not cause detectable lineshape effects; e.g., uniaxial diffusion with a restriction half-angle < 0.5 rad (30°) hardly influences the lineshape. Obviously, one should be careful to conclude the absence of motion from the absence of motional narrowing alone. In this range motional information can best be obtained from relaxation studies. Motions with larger amplitudes can significantly alter the lineshape. An intermediate amplitude range may be distinguished between 0.5 and 1.5 rad, where lineshape and transversal relaxation are sensitive to small changes in the amplitude. The third range consists of still larger amplitudes.

In this region lineshapes and transversal relaxation are insensitive to amplitude changes and restricted motion hardly can be distinguished from unrestricted motion.

A similar division can be made for motional frequencies as well. The slow-motion range contains low frequencies as compared with static linewidth and correlation times in the order of the transversal relaxation time T_{2e} or longer. In this region diffusion does not alter the lineshape in a detectable way and causes nonexponential relaxation. Typically the powder average decay of the echo $E(t, 0)$ is a function of Dt^3 and T_{2e} is inversely proportional to the cube root of the diffusion coefficient. In contrast, in the fast-motion region lineshapes are generally strongly narrowed and transversal relaxation is exponential. Within this frequency region the lineshape is dominated by the time-independent part of the chemical shift interaction and transversal relaxation is well described by the Redfield theory. In the intermediate region the time-dependent part of the chemical shift interaction cannot be neglected in lineshape calculations and the Redfield theory is not applicable. Other methods are necessary to simulate lineshapes and transversal relaxation.

The diffusion models discussed in this article serve to interpret the ^{31}P lineshapes and powder average decays measured for large virions in viscous gels. The application of these models on our NMR results obtained for M13 and TMV will be treated in a following article.

APPENDIX

Speeding up uniaxial diffusion simulations

An echo or free induction decay can be calculated from Eq. 18 for a series of t or τ values, respectively. After diagonalizing $\mathbf{M} = \mathbf{D}\Lambda\mathbf{D}^{-1}$ the calculation may proceed in a straightforward way

$$\sum_{i,j} (e^{\mathbf{M}(\tau+t)}e^{\mathbf{M}^*\tau})_{ij} = \sum_{i=1}^{N}\sum_{j=1}^{N}\sum_{k=1}^{N}\sum_{l=1}^{N}\sum_{m=1}^{N} \mathbf{D}_{ik}e^{\Lambda_{kk}(\tau+t)}\mathbf{D}^{-1}_{km}\mathbf{D}^*_{ml}e^{\Lambda^*_{ll}\tau}(\mathbf{D}^{-1}_{ij})^*. \quad (A1)$$

Due to the symmetry properties of matrix $\mathbf{M}$, matrix $\mathbf{D}$ can be orthogonalized by normalizing its columns, so that the inverse matrix $\mathbf{D}^{-1}$ can quickly be obtained by simple transposition. Still, however, the multiple sum in Eq. A1 for every t or τ value separately takes much computer time, which increases as the fifth power of the number of sites. Furthermore Eq. A1 also should be summed over many rotor orientations (θ, ψ_o) and internal chemical shift tensor orientations (β, γ). Therefore, speeding up the simulation is therefore essential for a practical use. A more efficient way is to calculate in a first step

$$A_{km} = D_{mk}\sum_{i=1}^{N} D_{ik}, \quad (A2)$$

and in the second step

$$B_m(\tau, t) = \sum_{k=1}^{N} A_{km}e^{\Lambda_{kk}(\tau+t)}. \quad (A3)$$

To simulate an echo, $B_m(\tau, t)$ is calculated for a specific value of τ and a series of t values and the echo is obtained from

$$\sum_{i,j} (e^{\mathbf{M}(\tau+t)}e^{\mathbf{M}^*\tau})_{ij} = \sum_{m=1}^{N} B_m(\tau, t)B^*_m(\tau, 0) \quad (A4)$$

To simulate a decay, $B_m(\tau, 0)$ is calculated for a series of τ values and the decay follows from

$$\sum_{i,j} (e^{\mathbf{M}\tau}e^{\mathbf{M}^*\tau})_{ij} = \sum_{m=1}^{N} |B_m(\tau, 0)|^2. \quad (A5)$$

Assuming that the rotors are randomly oriented in an isotropic powder and that the chemical shift tensors are also randomly oriented within every rotor separately (as may be the case for M13), Eqs. A4 and A5 still have to be summed over a large variety of rotor orientations (θ, ψ_o) and internal chemical shift tensor orientations (β, γ). It is well known that, for simulating static powder lineshapes, only part of the orientations within an isotropic powder has to be taken into account due to the symmetry of the chemical shift anisotropy (21). Likewise, symmetric properties of Eq. 13 reduce the number of rotor and tensor orientations that are actually needed in rotor diffusion simulations. Using the properties $d^2_{mm'}(\beta) = (-1)^{m-m'}d^2_{-m-m'}(\beta)$ and $d^2_{-mm'}(\beta) = (-1)^{m'} \times d^2_{mm'}(\pi - \beta)$ and combining the terms $\pm m'$, the anisotropic part of Eq. 13 may be rewritten as

$$\begin{aligned}
&\omega_0 d^2_{00}(\theta)[F_0 d^2_{00}(\beta) + 2F_2 d^2_{20}(\beta)\cos(2\gamma)] \\
&\quad + 2\omega_0 d^2_{10}(\theta)[F_0 d^2_{01}(\beta)\cos(\varphi) \\
&\quad + F_2(d^2_{21}(\beta)\cos(\varphi + 2\gamma) \\
&\quad - d^2_{21}(\pi - \beta)\cos(\varphi - 2\gamma))] \\
&\quad + 2\omega_0 d^2_{20}(\theta)[F_0 d^2_{02}(\beta)\cos(2\varphi) \\
&\quad + F_2(d^2_{22}(\beta)\cos(2\varphi + 2\gamma) \\
&\quad + d^2_{22}(\pi - \beta)\cos(2\varphi - 2\gamma))], \quad (A6)
\end{aligned}$$

where $\varphi = \psi + \alpha$. Eq. A6 shows that the chemical shift is invariant under the rotations $(\theta, \varphi) \rightarrow (\pi - \theta, \pi + \varphi)$, $(\beta, \varphi) \rightarrow (\pi - \beta, \pi + \varphi)$, $\gamma \rightarrow \pi + \gamma$, and $(\gamma, \varphi) \rightarrow (\pi - \gamma, 2\pi - \varphi)$. The diffusion operator (Eq. 14) is invariant under these rotations as well. Thus, if for rotor diffusion simulations φ is sampled from the whole interval $\langle 0, 2\pi \rangle$, the lineshape is sufficiently defined by θ, β, and γ taken from $\langle 0, \pi/2 \rangle$, which only represent one-sixteenth of all possible orientations.

This research was supported by the Netherlands Foundation of Biophysics with financial aid of the Netherlands Organization for Scientific Research (NWO).

Received for publication 30 November 1992 and in final form 23 February 1993.

REFERENCES

1. Kan, J. H., A. F. M. Cremers, C. A. G. Haasnoot, and C. W. Hilbers. 1987. The dynamical structure of the RNA in alfalfa mosaic virus studied by phosphorus-31 nuclear magnetic resonance. *Eur. J. Biochem.* 168:635–639.
2. Virudachalam, R., M. Harrington, J. E. Johnson, and J. L. Markley. 1985. Proton, carbon-13, and phosphorus-31 nuclear magnetic resonance studies of cowpea mosaic virus: detection and exchange of polyamines and dynamics of the RNA. *Virology.* 141:43–50.
3. Munowitz, M. G., C. M. Dobson, R. G. Griffin, and S. C. Harrison. 1980. On the rigidity of RNA in tomato bushy stunt virus. *J. Mol. Biol.* 141:327–333.

4. Bolton, P. H., G. Clawson, V. J. Basus, and T. L. James. 1982. Comparison of ribonucleic acid-protein interactions in messenger ribonucleoproteins, ribosomes, MS2 virus, and Qβ virus examined via phosphorus-31 nuclear magnetic resonance relaxation. *Biochemistry.* 21:6073–6081.
5. Cross, T. A., S. J. Opella, G. Stubbs, and D. L. D. Caspar. 1983. Phosphorus-31 nuclear magnetic resonance of the RNA in tobacco mosaic virus. *J. Mol. Biol.* 170:1037–1043.
6. Tsang, P., and S. J. Opella. 1986. Pf1 virus particle dynamics. *Biopolymers.* 25:1859–1864.
7. DiVerdi, J. A., and S. J. Opella. 1981. Phosphorus-31 nuclear magnetic resonance of fd virus. *Biochemistry.* 20:280–284.
8. Cross, T. A., P. Tsang, and S. J. Opella. 1983. Comparison of protein and deoxyribonucleic acid backbone structures in fd and Pf1 bacteriophages. *Biochemistry.* 22:721–726.
9. Campbell, R. F., E. Meirovitch, and J. H. Freed. 1979. Slow-motional NMR line shapes for very anisotropic rotational diffusion. Phosphorus-31 NMR of phospholipids. *J. Phys. Chem.* 83:525–533.
10. Dufourc, E. J., C. Mayer, J. Stohrer, G. Althoff, and G. Kothe. 1992. Dynamics of phosphate head groups in biomembranes. Comprehensive analysis using phosphorus-31 nuclear magnetic resonance lineshape and relaxation time measurements. *Biophys. J.* 61:42–57.
11. Bolton, P. H., and T. L. James. 1979. Molecular motions in RNA and DNA investigated by phosphorus-31 and carbon-13 NMR relaxation. *J. Phys. Chem.* 83:3359–3366.
12. Opella, S. J., W. B. Wise, and J. A. DiVerdi. 1981. Deoxyribonucleic acid dynamics from phosphorus-31 nuclear magnetic resonance. *Biochemistry.* 20:284–290.
13. Edsall, J. T. 1953. Size, shape and hydration of protein molecules. *In* The Proteins. H. Neurath and K. Bailey, editors. Academic Press Inc., New York. 549–686.
14. Magusin, P. C. M. M., and M. A. Hemminga. 1993. Analysis of 31P NMR lineshapes and transversal relaxation of bacteriophage M13 and Tobacco Mosaic Virus. *Biophys. J.* 64:1861–1868.
15. Freed, J. H., G. V. Bruno, and C. F. Polnaszek. 1971. Electron spin resonance line shapes and saturation in the slow motional region. *J. Phys. Chem.* 75:3385–3399.
16. Spiess, H. W., and H. Sillescu. 1981. Solid echoes in the slow-motion region. *J. Magn. Reson.* 42:381–389.
17. Pauls, K. P., A. L. MacKay, O. Soederman, M. Bloom, A. K. Tanjea, and R. S. Hodges. 1985. Dynamic properties of the backbone of an integral membrane polypeptide measured by deuteron NMR. *Eur. Biophys. J.* 12:1–11.
18. Alam, T. M., and G. P. Drobny. 1991. Solid-state NMR studies of DNA structure and dynamics. *Chem. Rev.* 91:1545–1590.
19. Abragam, A. 1961. The Principles of Nuclear Magnetism. Oxford University Press, London. 599 pp.
20. Edmonds, A. R. 1960. Angular Momentum in Quantum Mechanics. Princeton University Press, Princeton, NJ. 146 pp.
21. Haeberlen, U. 1976. High Resolution NMR in Solids: Selective Averaging. *Adv. Magn. Reson. Suppl. 1* (J. S. Waugh, editor). Academic Press, New York. 208 pp.
22. Slichter, C. P. 1978. Principles of Magnetic Resonance. Springer-Verlag, Berlin. 397 pp.
23. Hull, W. E., and B. D. Sykes. 1975. Fluorotyrosine alkaline phosphatase: internal mobility of individual tyrosines and the role of chemical shift anisotropy as a 19F nuclear spin relaxation mechanism in proteins. *J. Mol. Biol.* 98:121–153.
24. Wittebort, R. J., and A. J. Szabo. 1978. Theory of NMR relaxation in macromolecules: restricted diffusion and jump models for multiple internal rotations in amino acid side chains. *J. Chem. Phys.* 69:1722–1736.
25. Woessner, D. E., B. S. Snowden, Jr., and G. H. Meyer. 1969. Calculation of N.M.R. free induction signals for nuclei of molecules in a highly viscous medium or a solid-liquid system. *J. Chem. Phys.* 51:2968–2976.